Effect of Microstructure on Corrosion Behavior of TiN Hard Coatings Produced by Two Grid-Attached Magnetron Sputtering

†Jung Gu Kim and Woon Suk Hwang[1]

Department of Advanced Materials Engineering, Sungkyunkwan University
300 Chunchun-Dong, Jangan-Gu, Suwon 440-746, Korea
[1]School of Materials and Science Engineering, Inha University
253 Yonghyun-Dong, Incheon 452-752, Korea

The introduction of two-grid inside a conventional process system produces a reactive coating deposition and increases metal ion ratio in the plasma, resulting in denser and smoother films.

The corrosion behaviors of TiN coatings were investigated by electrochemical methods, such as potentiodynamic polarization test and electrochemical impedance spectroscopy (EIS) in deaerated 3.5% NaCl solution. Electrochemical tests were used to evaluate the effect of microstructure on the corrosion behavior of TiN coatings exposed to a corrosive environment. The crystal structure of the coatings was examined by X-ray diffractometry (XRD) and the microstructure of the coatings was investigated by scanning electron microscopy (SEM) and transmission electron spectroscopy (TEM).

In the potentiodynamic polarization test and EIS measurement, the corrosion current density of TiN deposited by two grid-attached magnetron sputtering was lower than TiN deposited by conventional magnetron type and also presented higher R_{ct} values during 240 h immersion time. It is attributed to the formation of a dense microstructure, which promotes the compactness of coatings and yields lower porosity.

Keywords : magnetron sputtering, porosity, packing factor, equivalent circuit, EIS

1. Introduction

One of the main tasks of hard coatings deposited by physical vapor deposition (PVD) is to enhance the lifetime of industrial applications. This improvement requires coatings with good adhesion, dense structure and chemical stability. Transition metal nitride coatings produced by magnetron sputtering techniques have been studied intensively since the beginning of the 1980s.

Titanium nitride (TiN) coatings prepared by PVD techniques exhibit good corrosion resistance, and their appearances are an attractive gold-like color. Corrosion behavior was characterized using potentiodynamic polarization test and EIS.[1,2] It has been reported that in certain corrosive environments, the service life of TiN coatings can be increased by reducing porosity. This porosity, such as pores, pinholes and voids, acts as pathways for rapid corrosion, allowing the substrate underneath to be corroded. This may finally cause the coating to flake away,

leading to a complete failure of the coating.[3] Porosity is closely related to the microstructure and packing factor of coatings, and is inversely proportional to the film density. The positive effects of greater packing factor act on inhibiting the passage of the corrosive electrolyte to the substrate and reducing the localized corrosion kinetics. The higher the packing factor, the higher the compactness of microstructure.

The aim of the present paper is to study the effect of microstructure on the corrosion properties with and without two grid-attached magnetron sputtering.

2. Experimental methods

2.1 Material preparation and coating deposition

Composition of the high speed steel (HSS, AISI D2) was 5.0% Cr, 1.3% Mo, 1.0% V, 1.0% Si, 0.5% Mn, 0.37% C, 0.03% P, 0.03% S and 90.77% Fe. Samples with diameter 12 mm were cut from 4 mm thick plate. All samples were ground to 2000 grit, cleaned in distilled water and dried with ethyl alcohol. The new magnetron
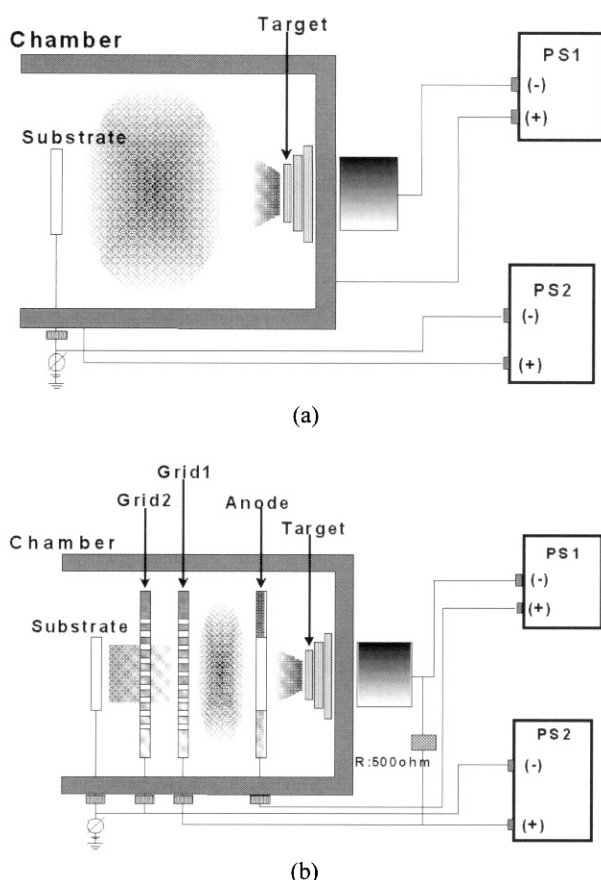
†Corresponding author: kimjg@skku.ac.kr

Fig. 1. Schematic diagrams of the experimental apparatus : (a) conventional, (b) two grid-attached magnetron type.

Table 1. Depositional conditions.

Base pressure	3×10^{-5} Torr
Working pressure	3×10^{-3} Torr
Distance between target and substrate	70 mm
Target current	0.5 A
Substrate bias voltage	0, -100, -150 V
Coating thickness	1 μm

rinsed with isopropanol and dried in hot air. Experimental conditions for DC magnetron sputter deposition are shown in Table 1.

2.2 Corrosion testing

The three-electrode electrochemical system was employed. A saturated calomel electrode (SCE) and a pure graphite electrode were used as reference and counter electrodes, respectively. The specimen was the working electrode. The exposed surface area was 0.25 cm^2. All of the potentials reported were measured with respect to the saturated calomel electrode. Electrochemical analyses included dc polarization and ac impedance spectroscopy techniques. DC measurements were performed with an EG&G PAR 263A potentiostat. A stable open-circuit potential (OCP) was usually obtained within 4 h. A scan rate of 0.166 mVs^{-1} was used in the dc analyses.

EIS data were collected over a frequency range of 1 mHz to 100 kHz. Alternating current (AC) amplitudes of 10 mV were applied. The evolution of the impedance spectra as a function of the immersion time was investigated. The impedance data were analyzed by the IM6e analysis software (THALES) program which used a nonlinear least square (NLLS) fitting. The equivalent circuits were used to carry out the fitting of the experimental EIS spectra collected at various intervals within the exposure of 10 days. Experiments were conducted at the OCP.

Electrochemical measurements were made at room temperature in deaerated 3.5% NaCl solution. The solution was prepared from analytical reagent grade chemicals and de-ionized water.

2.3 Porosity

Existence of porosity as pathways through the coating accelerated the localized corrosion. Owing to the generation of corrosion resulting from the contact between the substrate and the corrosive environment, the porosity measurement in the coating is essential to determine the corrosion-resistant coating. Determination of porosity is difficult because of the small size of the defects. By using electrochemical measurements, porosity can be estimated

system used for depositing TiN coatings is shown in Fig. 1. A novel design, the incorporation of two titanium grids and one anode embedded within the deposition chamber, was developed to produce ion particles which were accelerated toward the substrate. When Ar gas is introduced into chamber through the gas inlet, it is excited by the DC power supply to form plasma. The first grid (positive) is connected to the target via a resistor of 500 ohms to ease plasma beam formation. The second electrode (negative) and the substrate are connected to the earth potential. Thus, an accelerating electric field for positive ions can be established by a second DC power supply between the first and second grids. Deposition methods used in our experiment are similar to a classical ion source. The target, grid electrodes and anode correspond to the cathode, anode and extraction electrode of the classical ion source.[4] This equipment may also be adapted to the conventional system by removing the grids and anode. In the case of the conventional system, by applying bias to the substrate, ions can be accelerated toward the substrate. Circular Ti target of 2 inch diameter was used. Prior to deposition, specimens were cleaned by acetone in an ultrasonic bath, then

from electrochemical values. Matthews et al.[5] established an empirical equation to estimate the porosity (F) of the coating.

$$F = \frac{R_{pm(substrate)}}{R_{p(coating - substrate)}} \times 10^{-|\Delta E_{corr}/\beta_a|}$$

where F is the total coating porosity, R_{pm} the polarization resistance of the substrate, R_p the measured polarization resistance of the coated steel systems. ΔE_{corr} is the difference of the corrosion potential between the coating and the substrate, and β_a the anodic Tafel slope of the substrate.

Also, the porosity is related to the packing factor. The packing factor reflects the denseness of a coating. A quantitative measurement of the effect of defects (pores, pinholes) on coating density is the packing factor (P). Using the porosity, the packing factor can be determined by the following.[6]

$$P = \frac{\text{Volume of solid}}{\text{Total volume of coating (solid + pores)}}$$

The volume of solid is the exposed volume except the volume of pores into corrosive environment.

2.4. Surface analyses

XRD was conducted to collect crystallographic information such as crystal structure and preferred orientation. Mitutoyo surface roughness tester (Surftest 211 series 178) was used in the measurement of surface roughness. Cross-sectional SEM and TEM observations were conducted to investigate the morphology and microstructure of the coating. The TiN film thickness was measured from the observation of SEM.

3. Results and discussion

3.1 Coating characterization

The crystal structure was measured by XRD. To optimize the properties of the TiN coated steels, the effect of the bias voltages on the structure and phase was investigated. Experiments were carried out by applying the bias voltage in the range of 0 to -150 V. Fig. 2 shows XRD patterns of the coatings as a function of magnetron type and bias voltage. It was observed that the magnetron type and the degree of bias applied to the substrate during TiN deposition strongly influenced the crystal orientation of the coatings. The microstructure of TiN coatings prepared by the two grid-attached magnetron types appears
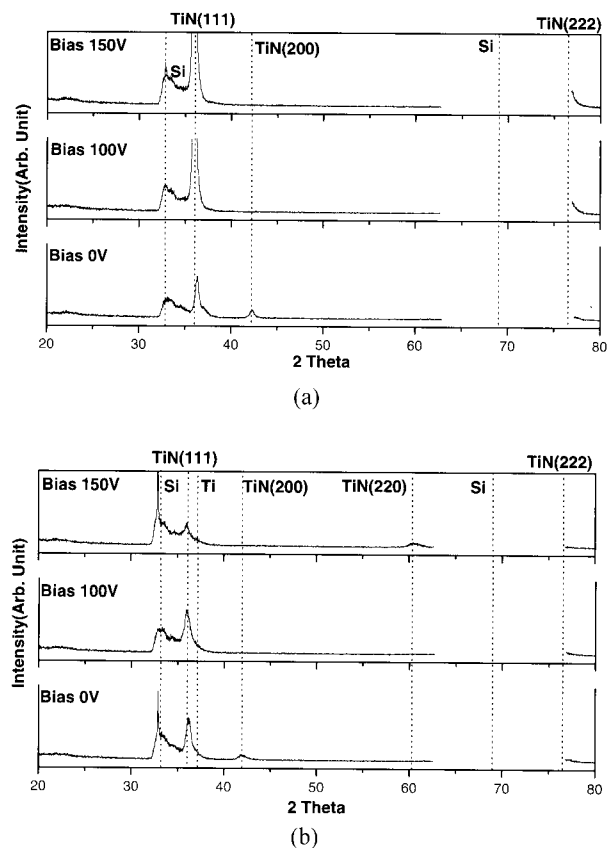

Fig. 2. XRD patterns of TiN films coated on Si wafer by conventional and two grid-attached magnetron as increasing bias voltage : (a) conventional, (b) two grid-attached magnetron type.

to be quite different from those created by conventional magnetron type. The TiN coatings deposited using the conventional magnetron type exhibit the preferential orientation of (222) and (111) as the bias voltage increased. On the other hand, for the two grid-attached magnetron, the TiN coatings exhibit highly preferred (111) orientation with increasing bias voltage.[4] As the bias voltage increases, the diffracted intensity of TiN (111) is decreased. The lower intensity of the peaks indicates that the size of crystallites has reduced.[7]

From the above results, an optimized condition for deposition can be observed for TiN coatings with increasing ion mobility (ion density) through grids as well with increasing the substrate bias voltage (ion energy). Increasing either parameter leads to enhance the ion bombardment of the growing film and the overall re-sputter rate of the condensed atoms. Also, the surface roughness of the TiN coating deposited by two grid-attached magnetron type at bias voltage of -100 V is lower than others coatings, as shown in Fig. 3. Thus, an optimized bias voltage for TiN deposition with and without two grid-attached type is -100 V.
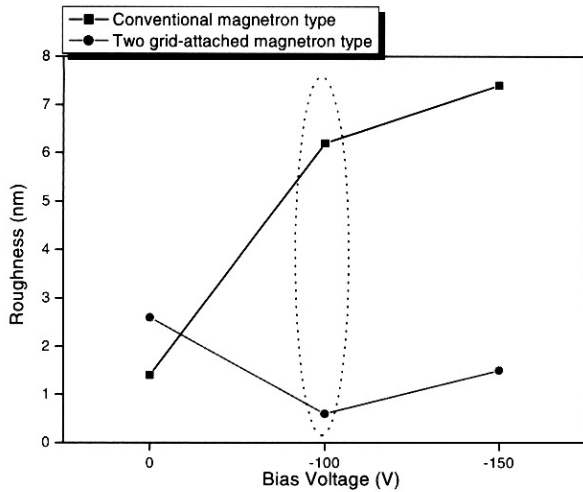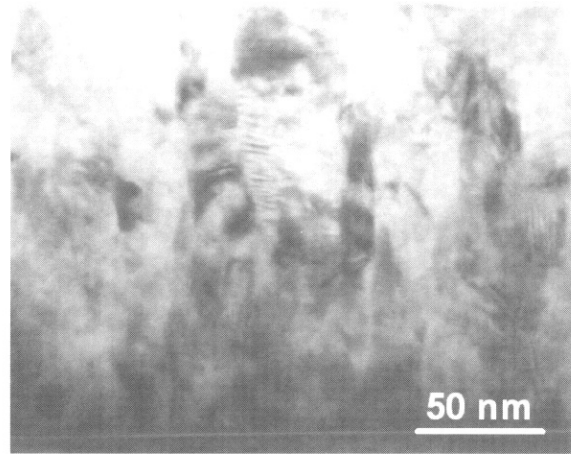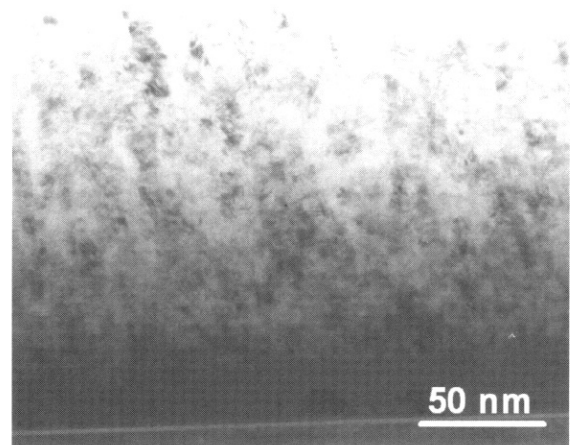
Fig. 3. Surface roughness of TiN coatings by conventional and two-grid magnetron as increasing bias voltage.
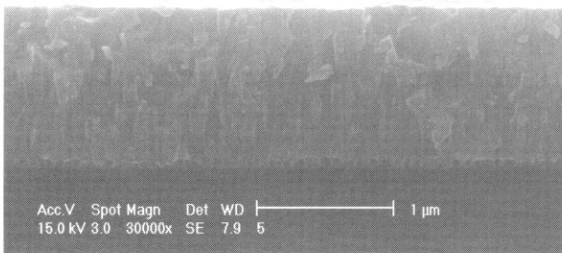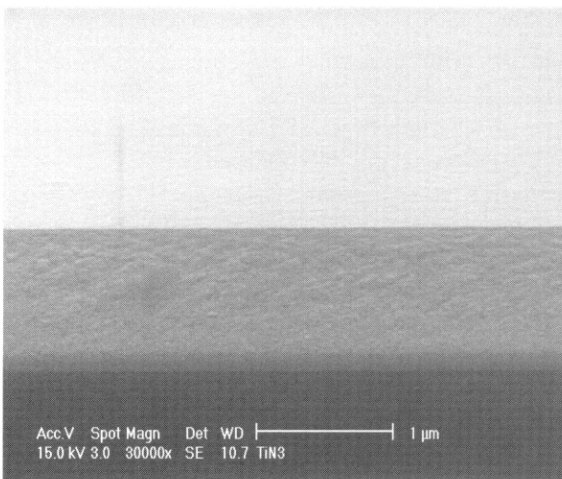

(a)

(a)

(b)

Fig. 5. Cross-sectional TEM images of TiN coatings: (a) conventional, (b) two grid-attached magnetron type.


(b)

Fig. 4. Cross-sectional images of TiN coatings coated on Si wafer: (a) conventional, (b) two grid-attached magnetron type.

3.2 Surface and cross-sectional structure

The surface and cross-sectional micrographs shown in Fig. 4(a-b) illustrate the microstructure of the different films. TiN coating deposited by conventional magnetron type exhibited columnar grains (Fig. 4(a)). In contrast, TiN coating deposited by two grid-attached magnetron type was a microcolumnar and smoother top surface, as shown in Fig. 4(b). This is due to ionic bombardment of the surface of the growing film, which is intensive enough to suppress columnar growth. Smoothing of the surface is due to increased preferential resputtering of the column tops with increased ion bombardment.[8] TEM was used to complement the structural characterization, as shown in Fig. 5. The cross-sectional TEM micrographs indicated that TiN coating by conventional process was composed

of columnar structures, as shown in Fig. 5(a). TiN coating using two grid-attached magnetron type was fine-grained polycrystalline structures. A high nucleation density allows a complete coating of smaller grains to form and leads to a smoother coating surface than those grown at lower nucleation densities. These results are consistent with SEM observations.

Fig. 6(a-b) shows the surface morphologies of the specimens after 240 h impedance measurements. Fig. 6(a)
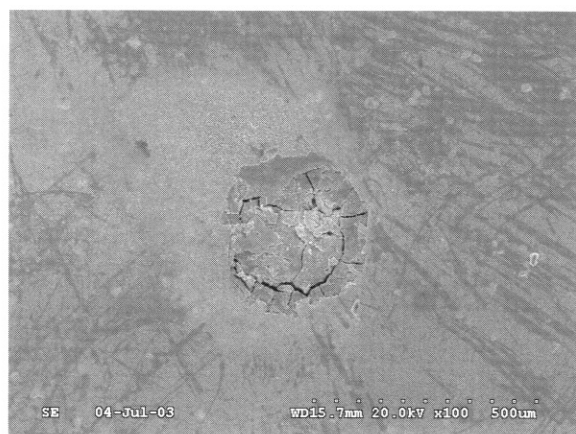
(a)
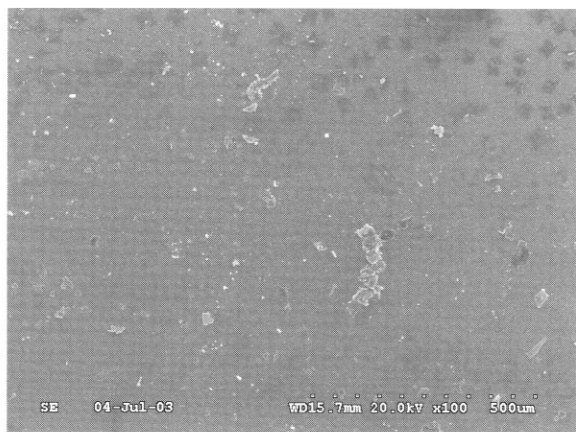
(b)

Fig. 6. Corroded surface appearances of TiN coatings after impedance measurement in a 3.5% NaCl electrolyte: (a) conventional, (b) two grid-attached magnetron type.

shows the localized damage with extensive intergranular attack of the substrate. However, it was noticed that only a slight deterioration for the TiN coating deposited by two grid-attached magnetron type had developed. During the exposure time, no localized corrosion could be observed, as shown in Fig. 6(b).

3.3 Corrosion properties

The results obtained from the potentiodynamic polarization tests are presented in Table 2 and Fig. 7. From these curves, the corrosion current density for TiN deposited by conventional magnetron type was 8.451 μA/cm^2 and relatively higher than that of 0.6267 μA/cm^2 for TiN deposited by two grid-attached magnetron type. An increase in the polarization resistance compared with the uncoated steel substrate was observed for all coated samples, as indicated by lower corrosion current densities. An improved corrosion resistance can be attributed to the densification of the microstructure due to ion bombardment during film growths. The lowest corrosion current density is obtained for TiN deposited by two grid-attached magnetron type. A combination of the equation of A. Matthews et al.[5] and electrochemical determinations gives a porosity of 0.1466% for TiN deposited by conventional magnetron type and 0.0084% for TiN deposited by two grid-attached magnetron type. The porosity is higher in
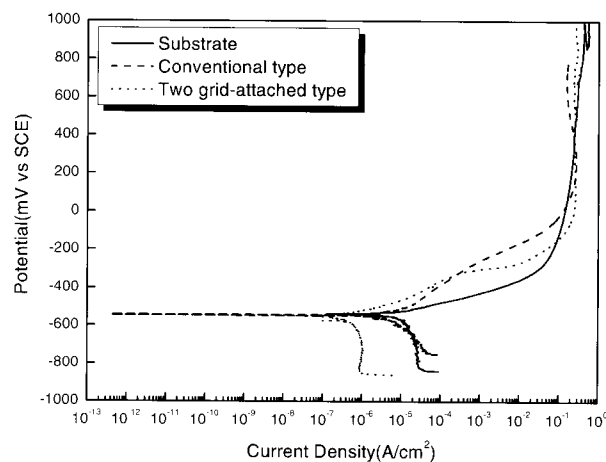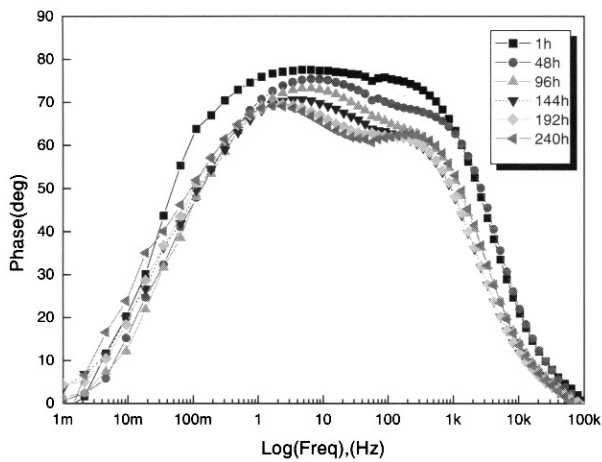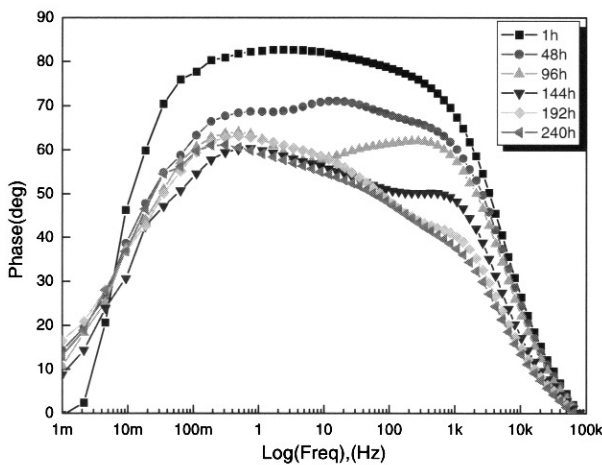

Fig. 7. Results of potentiodynamic polarization tests.

Table 2. Results of electrochemical experiments.

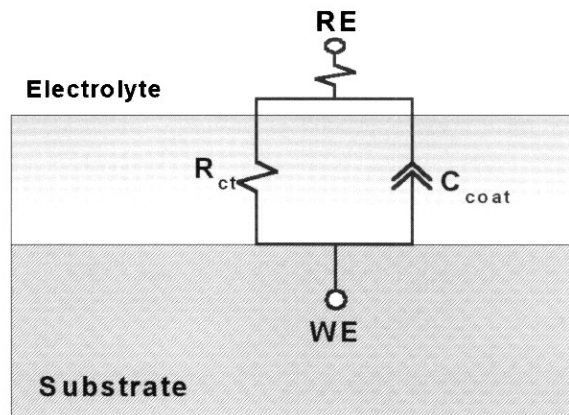| Specimen	E_{corr} (mV)	i_{corr} (μA/cm^2)	β_a (V/decade)	β_c (V/decade)	R_p ($\times 10^3$ Ωcm^2)	Porosity (%)	Packing factor
Substrate	-541.9	14.69	0.0960	0.2231	1.988	-	-
Conventional type	-545.7	8.451	0.1478	0.271	1,237.24	0.1466	0.9985
Two-grid type	-551	0.6267	0.0971	0.6611	18,845.11	0.0084	0.9999

(a)

(b)

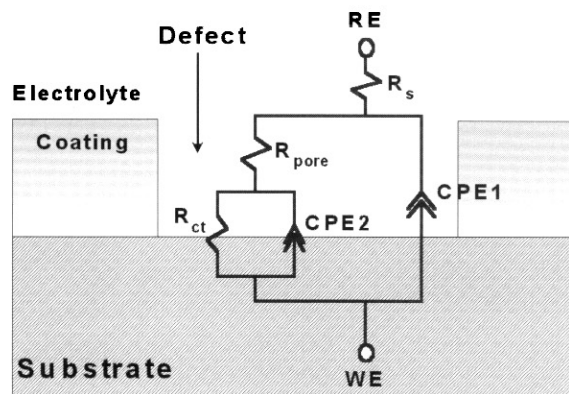**Fig. 8.** Bode plots for EIS data of TiN coatings for different exposure times: (a) conventional type, (b) two grid-attached magnetron type.

(a)

(b)

Fig. 9. Electrical model for the interpretation of impedance data: (a) one time constant, (b) two time constants.

the TiN deposited by conventional magnetron type than in the TiN deposited by two grid-attached magnetron type. Also, the packing factor is associated with the denseness of the coating. The lower the calculated porosity, the higher the packing factor. The beneficial effects of greater packing factor act on inhibiting the passage of the corroding solution to the substrate and reducing the localized corrosion kinetics. The packing factors obtained are situated between 0.9985 and 0.9999, as shown in Table 2.

The EIS spectra are shown in Bode plots of the phase angle as a function of the logarithm of the frequency. Bode plots of the TiN-coated steel immersed for different periods are shown in Fig. 8. Table 3 summarizes the best-fitting values. These impedance results could be fitted to the model circuit of Fig. 9. The equivalent circuit consists of the following elements : For the case of one time constant (Fig. 9(a)), the equivalent circuit consisted

of a solution resistance (R_s) and a coating capacitance (C_{coat}) related to the nonideal capacitive behavior of the coating in parallel with the charge transfer resistance (R_{ct}). For the two time constants (Fig. 9(b)), the equivalent circuit consists of the following elements; R_s corresponds to the solution resistance and C_{pore} is the capacitance of the coating including pores in the outerlayer coating. R_{pore} is the pore resistance resulting from the formation of ionic conduction paths across the coating. C_{coat} is the capacitance of the coating within the pit and R_{ct} is the charge transfer resistance of the substrate/coating. The deviation of the impedance from pure capacitance behavior can be attributed to the inhomogeneity in the coating system and nonuniform diffusion.[9] There is some deviation of the data at several low frequency points. This can be attributed to the behavior of constant phase element (CPE). It can also be described in terms of a distribution of relaxation times.[10]

$$Z_{CPE} = Z_0(j\omega)^{-n}$$

Table 3. Electrochemical parameters obtained by equivalent simulation.

Exposure Time (hr)		R_s (Ω cm²)	CPE1		R_{pore} *R_{ct}(Ω cm²)	CPE2		R_{ct} ($\times 10^3$ Ω cm²)	** WSS
			C_{pore}, *C_{coat} ($\times 10^{-6}$F/cm²)	n (0-1)		C_{coat} (F/cm²)	n (0-1)		
1	C1	7.102	7.102	0.8655	134.3				5.4
	C2	7.753	7.753	0.905	476.6				5.6
48	C1	9.382	9.382	0.8288	59.56				0.7
	C2	8.52	8.52	0.7876	198				0.6
96	C1	10.66	10.66	0.8074	42.28				0.6
	C2	9.831	9.831	0.7225	7.355	125.4	1	71.42	0.7
144	C1	11.42	11.42	0.78	46.51				1.7
	C2	11.14	11.14	0.7136	7.521	209	1	48.75	0.9
192	C1	12.25	12.25	0.7714	18.9	132.4	1	19.92	0.7
	C2	16.17	16.17	0.6738	0.882	87.35	1	26.58	0.9
240	C1	13.37	13.37	0.7	17.96	124.9	1	17.93	1.6
	C2	19.58	19.58	0.7237	0.091	18.11	0.7112	23.99	0.6

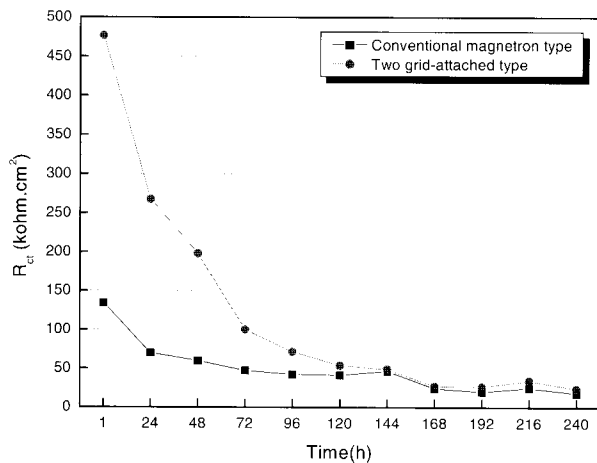*C1: conventional type, C2: two grid-attached magnetron type.

Fig. 10. Calculated charge transfer resistance for the TiN coatings as a function of the exposure time.

where Z_o is the adjustable parameter used in the nonlinear least squares fitting, ω is angular frequency and the factor n, defined as a CPE power, is an adjustable parameter that always lies between 0.5 and 1, which can be obtained from the slope of [Z] on the Bode plot.

Fig. 8 shows that the modifications occur according to the degradation of the coating. Initially, one time constant was clearly distinguished, but as exposure time increased, it tended to present two time constants. With increasing immersion time, the high frequency part decreases whereas the low frequency limit of the diagrams remains unchanged. The high frequency part of the diagram can be attributed to the properties of the coating and the decrease

of the high frequency part is related to electrolyte and ions penetration into the coating.[11] The equivalent circuit enabled the parameter values for the individual elements to be determined with a least-squares analysis. R_{ct} was measured after different immersion periods and the results were presented in Fig. 10. The values of R_{ct} decreased steadily with immersion time. This phenomenon is in agreement with an increase in the number of pores, which increase the area in contact with the electrolyte. For TiN coating deposited by two grid-attached magnetron type, R_{ct} values are much higher than the TiN coating deposited by conventional magnetron type. This provided an evidence of the effective barrier characteristics. After 192 h of immersion, the impedance of coating deposited by two grid-attached magnetron sputtering showed a small rise, which was probably due to corrosion products plugging the pores and increasing the resistance pathway. As the structure was compacted, the driving force for electrolyte penetration through coatings decreased.

4. Conclusions

1) The cross-sectional SEM and TEM morphologies of the TiN coatings deposited by two grid-attached magnetron type showed a distinct and dense structure.

2) In the potentiodynamic polarization test, the corrosion current density of TiN coating deposited by two grid-attached magnetron type was lower than TiN coating deposited by conventional magnetron type. This is consistent with the results of EIS measurement. For two types

of coatings, the value of R_{ct} decreased under the effect of ion diffusion through defects. During the immersion time, the R_{ct} value of TiN coating deposited by two grid-attached magnetron sputtering type was high, showing the good corrosion protection properties

3) After the 240 h immersion time, it was observed that TiN coating deposited by two grid-attached magnetron type had a slight deterioration. These results are consistent with the porosity and packing factor calculated by potentiodynamic polarization test.

Acknowledgments

References

1. C. Liu, Q. Bi, A. Leyland, and A. Matthews, *Corr. Sci.*, **45**, 1243 (2003).
2. B. Elsener, A. Rota, and H. Böhni, *Materials Science Forum* **44-45**, 29 (1989).
3. L. Cunda, M. Andrtschky, L. Rebouta, and K. Pishow, *Surf. Coat. Technol.*, **116-119**, 1152 (1999).
4. Min J. Jung, Kyung H. Nam, Leonid R. Shaginyan, and Jeon G. Han, *Thin Solid Films*, **435**, 145 (2003).
5. B. Matthes, E. Broszeit, J. Aromaa, H. Ronkainen, S.P. Hannula, A. Leyland, and A. Matthews, *Surf. Coat. Technol.* **49**, 489 (1991).
6. Milton Ohring, The Materials Science of Thin Films, Academic Press, San Diego, p. 233 (1992).
7. F. Vacandio, Y. Massiani, P. Gravier, and A. Garnier, *Surf. Coat. Technol.*, **92**, 221 (1997).
8. H. Paritong, M. Lembke, D.B. Lewis, and W.-D. Münz, *Surf. Coat. Technol.*, **116-119**, 1145 (1999).
9. J.Ross Macdonald, Impedance Spectroscopy, New York, NY: John Wiley & Sons, p. 91 (1987).
10. S.Rudenja, C. Leygraf, J. Pan, P. Kulu, E. Talimets, and V. Miki, *Surf. Coat. Technol.*, **114**, 129 (1999).
11. K. Bonuel, C. Le Pen, and N. Pébère, *Electrochimica Acta*, **44**, 4257 (1999).